Synthesis and Characterization of Uranium(IV)-Bearing Members of the [NZP] Structural Family

H. T. Hawkins,*,†,§ D. R. Spearing,† D. K. Veirs,† J. A. Danis,‡ D. M. Smith,‡ C. D. Tait,‡ and W. H. Runde‡

Nuclear Materials Technology and Chemical Science and Technology Divisions, Los Alamos National Laboratory, Los Alamos, New Mexico 87545

M. N. Spilde

Department of Earth and Planetary Sciences/Institute of Meteoritics, The University of New Mexico, Albuquerque, New Mexico 87131

B. E. Scheetz

Materials Research Laboratory, The Pennsylvania State University, University Park, Pennsylvania 16802

Received April 12, 1999. Revised Manuscript Received August 3, 1999

The sodium dizirconium tris(phosphate) structural family ([NZP]) includes compounds that may be represented by the general formula $M'M''_{1-3}A_2(PO_4)_3$. The ability of $KZr_2(PO_4)_3$, a member of the [NZP] structural family, to accommodate U(IV) on the octahedrally coordinated A site has been demonstrated for compounds in the series $KZr_{2-x}U_x(PO_4)_3$ ($0 \le x \le 0.20$). $KU_2(PO_4)_3$, the end member of the series, was found to adopt a monoclinic structure with 9-fold coordination of U(IV) that does not belong to the [NZP] family. The compounds were prepared from sol−gel derived precursors in an argon environment. X-ray microanalyses indicated that the precursor powders had reacted fully to produce compounds of the expected stoichiometries. Rietveld refined X-ray powder diffraction data of $KZr_{2-x}U_x(PO_4)_3$ ($0 \le x \le 0.20$) confirmed a rhombohedral ($R\bar{3}c$) structure and suggested random occupation of the A site by U/Zr. The presence of U(IV) was established by comparison of the UV/vis spectra of $KZr_{2-x}U_x(PO_4)_3$ ($0 \le x \le 0.20$) with those of other U(IV) phosphates including $KU_2(PO_4)_3$. The Rietveld refined data show an increase in the volume of the $R\bar{3}c$ cell with increasing values of x. The structure of $KU_2(PO_4)_3$, determined from Rietveld refinement of powder X-ray diffraction data, is monoclinic (space group $C2/c$, $Z = 4$) with unit cell parameters $a = 17.4705(4)$ Å, $b = 6.75408(13)$ Å, $c = 8.02522(17)$ Å, $\beta = 102.0189(17)°$, and $V = 926.196(34)$ Å^3. The final indicators of the quality of the Rietveld refinement were $R_{wp} = 14.07\%$, $R_e = 10.02\%$, and $R_F = 3.78\%$.

Introduction

Potassium dizirconium tris(phosphate) ($KZr_2(PO_4)_3$) is a member of the $NaZr_2(PO_4)_3$ structural family ([NZP]). Members of this structural family possess desirable properties that would permit their application as host materials for the actinides.[1−3] These properties include negligible thermal expansion,[4−6] compositional flexibility,[7−9] high thermal stability, and resistance to radiation damage,[10] and they are attributed to the three-dimensional [NZP] structure. However, the ability of the [NZP] framework to accommodate actinides such as Th(IV), U(IV), or Pu(III/IV) in solid solution has not been rigorously examined. Herein we examine the effects of U(IV) substitutions on the [NZP] unit cell.

The [NZP] structure, which may be represented by the general formula $M'M''_{1-3}A_2(PO_4)_3$, is a three-dimensional anionic framework of strongly bonded $[A^n{}_2(PO_4)_3]^{(2n-9)}$ units made up of corner-sharing AO_6 octahedra and PO_4 tetrahedra. The $[A^n{}_2(PO_4)_3]^{(2n-9)}$ units are linked to form ribbons along the c axis of the unit cell; PO_4 tetrahedra connect the ribbons along the a axis. For an $[A^n{}_2(PO_4)_3]^{(2n-9)}$ anionic framework in

* To whom correspondence should be addressed.
† Nuclear Materials Technology Division.
‡ Chemical Science and Technology Division.
§ Graduate student, Intercollege Materials Research Program, The Pennsylvania State University, University Park, PA.

(1) Roy, R.; Vance, E. R.; Alamo, J. *Mater. Res. Bull.* **1982**, *17*, 585.
(2) Scheetz, B. E.; Agrawal, D. K.; Breval, E.; Roy, R. *Waste Manage.* **1994**, *14*, 489.
(3) Hawkins, H. T.; Scheetz, B. E.; Guthrie, G. D. In *Scientific Basis for Nuclear Waste Management*; Gray, W. J., Triay, I. R., Eds.; Materials Research Society: Boston, MA, 1997; Vol. 465, p 387.
(4) Lenain, G. E.; McKinstry, H. A.; Limaye, S. Y.; Woodward, A. *Mater. Res. Bull.* **1984**, *19*, 1451.
(5) Agrawal, D. K.; Roy, R. *J. Mater. Sci.* **1985**, *20*, 4617.
(6) Oota, T.; Yamai, I. *J. Am. Ceram. Soc.* **1986**, *69*, 1.
(7) Alamo, J. *Solid State Ionics* **1993**, *63−65*, 547.
(8) Alami Talbi, M.; Brochu, R.; Parent, C.; Rabardel, L.; Le Flem, G. *J. Solid State Chem.* **1994**, *110*, 350.
(9) Kasthuri Rangan, K.; Gopalakrishnan, J. *Inorg. Chem.* **1995**, *34*, 1969.
(10) Kryukova, A. I.; Kulikov, I. A.; Artem'eva, G. Y.; Pechenevskaya, O. V.; Alferov, V. A. *Radiokhimiya* **1992**, *34*, 82.

10.1021/cm990209f CCC: $18.00
Published on Web 09/25/1999

which $n = 4$, charge balance is achieved through monovalent cation occupation of M′, large octahedral cavities that lie within the ribbons. Three additional sites that lie between the ribbons (M″) may be occupied by charge-balancing cations when the charge on the $[A^n{}_2(PO_4)_3]^{(2n-9)}$ anionic framework is increased (i.e. $n = 3$); however, in the rhombohedral ($R\bar{3}c$) structure of $NaZr_2(PO_4)_3$,[11,12] only M′ is occupied.[13]

Compounds in the [NZP] structural family share the same topology of polyhedral linkages ($[A^n{}_2(PO_4)_3]^{(2n-9)}$ units made up of corner-sharing AO_6 octahedra and PO_4 tetrahedra) within their anionic framework structures.[7] Compounds of similar stoichiometry ($M'A^{IV}{}_2(PO_4)_3$ where A = Th or Np) such as $KTh_2(PO_4)_3$, adopt a different structure type in which the coordination of A is 9-fold and the AO_9 and PO_4 polyhedra of the anionic framework share edges as well as corners.[14] Charge balance is achieved through cation occupation of interstitial sites of 8-fold coordination (M′); additional interstitial sites are not available for occupation by charge-balancing cations. Transition from the monoclinic $KTh_2(PO_4)_3$ structure to the rhombohedral [NZP] structure involves the breaking of bonds, suggesting incomplete solid solubility of $KTh_2(PO_4)_3$ in [NZP].

Conventional solid-state routes to $M'U_2(PO_4)_3$ (M′ = K, Na, or Li) single crystals have not been effective. This is due in part to the fact that the oxidation states of uranium and the other actinides are difficult to control under the high temperatures and extended periods of heat treatment required for the preparation of phase-pure [NZP] compounds. Whereas ThO_2 is stable in air at the high temperatures generally associated with ceramic processing, heating any of the uranium oxides under similar conditions (>800 °C) yields U_3O_8 in which uranium is present in more than one oxidation state.[15] Single crystals of $NaU_2(PO_4)_3$ containing dark cubic inclusions of U_3O_8 have been prepared by the reaction of constituent oxides/phosphates in molten B_2O_3 under reducing conditions (i.e., in graphite crucibles under flowing nitrogen)[16] and have been reported to form by the reaction of similar reagents in NaCl and B_2O_3 melts under oxidizing conditions.[17] Unit cell parameters for $M'U_2(PO_4)_3$ (M′ = K, Na, or Li) derived from least-squares analysis of powder X-ray diffraction (XRD) data have been reported;[16] however, precise structural information as well as spectroscopic confirmation of the presence of U(IV) is absent in this previous work.

The primary objective of this study was to examine the effect of U(IV) substitutions on the [NZP] unit cell to gain insight into the ability of the structure to accommodate large cations. We chose to investigate the potassium analogue of $NaZr_2(PO_4)_3$ because we hypothesized that the unit cell of $KZr_2(PO_4)_3$, with its greater cell volume, would more readily accommodate substitutions of the larger U^{4+} ($r = 0.89$ Å) for Zr^{4+} ($r = 0.72$ Å)[18] on the octahedrally coordinated A site. Given the problems associated with single-crystal synthesis of U(IV)-bearing [NZP] and $M'U_2(PO_4)_3$ compounds, we have applied the Rietveld method[19] to the X-ray powder structure refinement/solution of compounds in the series $KZr_{2-x}U_x(PO_4)_3$ ($x \leq 0.20$; $x = 2$) to obtain precise structural parameters.

Experimental Section

Synthesis. Compounds in the series $KZr_{2-x}U_x(PO_4)_3$ were prepared in stoichiometries consistent with the expected solid solubility limit of UO_2 in ZrO_2 ($x \leq 0.20$):[20] K:Zr:U:P of 1:2 − x:x:3 where $x = 0.02$, 0.08, 0.10, 0.20. The end members of the series ($x = 0$ and $x = 2$) were also prepared. Solutions of KNO_3 and $ZrOCl_2 \cdot 8H_2O$, prepared with high-purity (≥99.99%) reagents and reduced volumes of deionized H_2O, were mixed together under conditions of constant stirring at room temperature in accordance with the procedure described by Limaye.[21] Stoichiometric amounts of UCl_4 powder, prepared by the well-established procedure given in Hermann and Suttle,[22] were dissolved in reduced volumes of 0.01 M HCl. The UCl_4 solutions were then added to the $KNO_3/ZrOCl_2 \cdot 8H_2O$ solutions. $NH_4H_2PO_4$ solution was added dropwise to the solutions (pH = 2) to precipitate viscous, semitransparent gels that were dried under vacuum at 60 °C for 24 h. In the synthesis of $KU_2(PO_4)_3$, CH_3CH_2OH was added to force precipitation of the precursor gel.

The dried gels were ground in agate mortars, transferred to alumina or glassy carbon crucibles, and heat treated in a horizontal tube furnace under flowing ultrahigh purity argon to prevent the oxidation of U(IV) to U(VI), thus avoiding the formation of impurity phases such as U_3O_8 or $U(UO_2)(PO_4)_2$.[15,23] After an initial 24 h heat treatment at 400 °C, the samples were reground and returned to the furnace for a 24 h heat treatment at 950−1100 °C. Furnace heating and cooling rates were 3 °C·min^{-1} and 1 °C·min^{-1}, respectively. Additional 24−48 h heat treatments at 950−1100 °C were employed to ensure complete conversion of reactants to products.

X-ray Diffraction Data Collection. Powder XRD patterns were collected at room temperature with a Scintag XDS 2000 diffractometer (θ/θ geometry) using monochromatic Cu Kα_1 ($\lambda = 1.540\,598$ Å) radiation. Powder samples were deposited on zero-background quartz plates coated with silicone grease. Powder Si (NIST SRM 640b) or LaB_6 (NIST SRM 660) was added as an internal standard. The samples were rotated continuously during data collection so that the effects of preferred orientation on the data would be minimized. Data were recorded from 10 to 90° 2θ at 0.5°·min^{-1} for the purposes of indexing and assessment of phase purity. Indexing of the first 20 lines in each XRD pattern was performed with the program DICVOL91.[24] The General Structure Analysis System[25] (GSAS) was used in the application of the Rietveld method to the quantitative analysis of multiphase samples.[26]

For structure refinement of ($0 \leq x \leq 0.20$) compounds with the Rietveld method, powder XRD data were collected from

(11) Hagman, L.-O.; Kierkegaard, P. *Acta Chem. Scand.* **1968**, *22*, 1822.
(12) Hong, H. Y.-P. *Mater. Res. Bull.* **1976**, *11*, 173.
(13) Lucazeau, G.; Barj, M.; Soubeyroux, J. L.; Dianoux, A. J.; Delmas, C. *Solid State Ionics* **1986**, *18 & 19*, 959.
(14) Matković, B.; Prodić, B.; Šljukić, M.; Peterson, S. W. *Croat. Chem. Acta* **1968**, *40*, 147.
(15) Greenwood, N. N.; Earnshaw, A. *Chemistry of the Elements;* Pergamon Press: Ltd.: Cambridge, England, 1984.
(16) Keester, K. L.; Jacobs, J. T. *Ferroelectrics* **1974**, *8*, 657.
(17) Burnaeva, A. A.; Volkov, Y. F.; Kryukova, A. I.; Skiba, O. V.; Spiryakov, V. I.; Korshunov, I. A.; Samoilova, T. K. *Radiokhimiya* **1987**, *29*, 3.
(18) Shannon, R. D. *Acta Crystallogr.* **1976**, *A32*, 751.
(19) Rietveld, H. M. *J. Appl. Crystallogr.* **1969**, *2*, 65.
(20) Levin, E. M.; Robbins, C. R.; McMurdie, H. F. In *Phase Diagrams for Ceramists*; Reser, M. K., Ed.; The American Ceramic Society: Columbus, OH, 1964; p 70.
(21) Limaye, S. Y.; Agrawal, D. K.; Roy, R.; Mehrotra, Y. *J. Mater. Sci.* **1991**, *26*, 93.
(22) Hermann, J. A.; Suttle, J. F. In *Inorganic Syntheses*; Moeller, T., Ed.; McCraw-Hill Book Company, Inc.: New York, 1957; Vol. 5, p 143.
(23) Bénard, P.; Louër, D.; Dacheux, N.; Brandel, V.; Genet, M. *Chem. Mater.* **1994**, *6*, 1049.
(24) Boultif, A.; Louër, D. *J. Appl. Crystallogr.* **1991**, *24*, 987.
(25) Larson, A. C.; Von Dreele, R. B. *(GSAS) General Structure Analysis System*; Los Alamos National Laboratory Report LAUR 86-748; Los Alamos National Laboratory: Los Alamos, NM, 1986.
(26) Bish, D. L.; Post, J. E. *Am. Mineral.* **1993**, *78*, 932.

13 to 125° 2θ with a step of 0.02° 2θ and a counting rate of 14 s·step^{-1}. Two data sets were collected for the structure refinements of $KZr_2(PO_4)_3$ and $KU_2(PO_4)_3$: data were collected from 8 to 90° 2θ with a 0.02° 2θ step at 7 s·step^{-1} and from 70 to 139° 2θ with a 0.04° 2θ step at 14 s·step^{-1} on a sample of the compound mixed with LaB_6 as an internal standard. The two data sets were simultaneously refined and scaled appropriately. Unit cell parameters, atomic positions, thermal parameters, and fractional site occupancies were extracted from the data using GSAS. The GSAS subroutine DISAGL was used in the calculation of A−O and P−O bond distances and angles.

X-ray Microanalysis. The U/Zr molar ratio and homogeneity of phase-pure samples (as suggested by powder XRD data) was determined with a JEOL JXA 733 electron microprobe at the Department of Earth and Planetary Sciences/Institute of Meteoritics, University of New Mexico. The microprobe is equipped with 5 wavelength dispersive X-ray spectrometers (WDS) and an Oxford Instruments eXL II analytical system. Analyses were conducted at 15 kV and 20 nA with a spot size of 1 μm. Natural mineral and synthetic oxide standards from C. M. Taylor Corporation were used as calibration standards with 20 s counting times on each standard. Counting times on the samples were 20 s for major elements and 30−40 s for minor elements. A ZAF correction program from Oxford was used to reduce the raw data.

Spectroscopic Characterization. UV/vis spectra of powder samples were recorded on a Perkin-Elmer Lambda 19 spectrometer using a Labsphere RSA-PE-19 reflectance spectroscopy attachment. The resolution of the spectrometer is 2 nm. Data were collected from 300 to 1100 nm in 0.2 nm steps at 60 nm·min^{-1}.

Results

Our initial powder XRD data showed the $KZr_{2-x}U_x(PO_4)_3$ ($x \leq 0.20$) compounds prepared in either crucible type (alumina or glassy carbon) to be phase pure and isostructural with $KZr_2(PO_4)_3$. However, the XRD data indicated that alumina crucibles are necessary for the preparation of phase-pure $KU_2(PO_4)_3$, a dark green compound that was found to be isostructural with $KTh_2(PO_4)_3$.[16] XRD patterns of $KU_2(PO_4)_3$ prepared in glassy carbon crucibles revealed an impurity phase (15.1 wt % as determined by the Rietveld method) which was identified as UP_2O_7, uranium(IV) diphosphate.[27] The presence of UP_2O_7 suggests that under the conditions of heat treatment, glassy carbon crucibles both prevent oxidation of U(IV) to U(VI) and promote reduction of PO_4^{3-} to $P_2O_7^{4-}$.

Sample Homogeneity. Measurements of the U/Zr molar ratio in the powder samples indicated that the precursors reacted fully to produce compounds of the expected stoichiometries. Two of the samples contained particles of an UO_2-rich phase that appeared to be evenly distributed on the surfaces of the samples, occupying less than 1% of their surface areas. UO_2 as an impurity phase was not detected in the powder XRD pattern of either sample collected with Si as an internal standard. However, UO_2 ($Fm\bar{3}m$) and Si ($Fd\bar{3}m$) share the same Laue symmetry ($m\bar{3}m$) and have similar unit cell constants (5.445 and 5.43094(35) Å, respectively).[28] This structural similarity could give rise to peak overlap, particularly in the case of peak-width variations caused by differences in anisotropic strain broadening, or particle size broadening in the two phases. Rietveld refinement of the powder XRD data sets collected without internal standards did not reveal the presence of UO_2 or any other impurity phase, suggesting that the amount of the UO_2-rich phase in the samples is less than that detectable in a Rietveld quantitative analysis (approximately 1 wt %).[26]

Rietveld Study: U(IV) on A in $KA_2(PO_4)_3$. In the initial refinements of the powder XRD data for members of the series $KZr_{2-x}U_x(PO_4)_3$ ($x \leq 0.20$), the $R\bar{3}c$ crystal structure of $KZr_2(PO_4)_3$[29] was used as the starting model. The nominal U/Zr molar ratio was assumed to be randomly distributed on A and full occupancy of M′ by K^+ was postulated. The three crystallographically equivalent M″ sites at (x, 0, $^1/_4$) were assumed to be vacant. The histogram or phase fraction scale factors, background coefficients, sample displacement error, unit cell parameters, and Lorentzian components of the pseudo-Voigt coefficients adjusted for strain broadening and peak asymmetry[30] were refined first. Soft constraints were applied to the A−O and P−O distances based on reported values.[31−34] The atomic positions were then refined.

The molar ratio of U/Zr on A for $KZr_{2-x}U_x(PO_4)_3$ ($0 \leq x \leq 0.20$) was allowed to vary. The isotropic thermal parameters of all the atoms were then refined freely. Difference Fourier maps were examined throughout the course of each refinement. In the final stages of the refinements, the soft constraints were removed to test the refined structural models. There were negligible decreases in the values of R_F and χ^2; however, the resulting structural models were less realistic than those obtained with the applied soft constraints (i.e. A−O bond distances were unrealistically short at ∼2.001 Å). Comparison of the ratio of R_{wp} to R_e, the statistically expected R_{wp} ($R_e = R_{wp}/\sqrt{\chi^2}$), to that which would be obtained for a perfect refinement (1.0) indicates the quality of the refinements obtained with applied soft constraints: the ratios fall in the range of 1.2−1.4. A summary of the refinement results that includes the agreement factors, soft constraints, unit cell parameters, and refined values of x (U/Zr adjusted for stoichiometry) for members of the series $KZr_{2-x}U_x(PO_4)_3$ ($x \leq 0.20$) prepared in alumina crucibles is given in Table 1. Final observed, calculated, and difference XRD profiles for $KZr_{1.90}U_{0.10}(PO_4)_3$ are shown in Figure 1 as an example of the quality of the Rietveld refinements. Atomic positions and thermal parameters for $KZr_{2-x}U_x(PO_4)_3$, where $x = 0$, 0.02, 0.07, 0.10, and 0.20, are given in Tables 2−6, respectively.

$KU_2(PO_4)_3$ Structure Solution. The DICVOL91 indexing of the first 20 lines of the XRD pattern of $KU_2(PO_4)_3$ returned a monoclinic solution (cell $V = 925.99$ Å^3) with the following figures of merit:[35] $M_{20} = 34.5$ and $F_{20} = 68.3(0.0059, 50)$. Systematic absences in the

(27) Cabeza, A.; Aranda, M. A. G.; Cantero, F. M.; Lozano, D.; Martínez-Lara, M.; Bruque, S. *J. Solid State Chem.* **1996**, *121*, 181.
(28) Cooper, M. J. *Acta Crystallogr.* **1982**, *38*, 264.
(29) Šljukić, M.; Matković, B.; Prodić, B.; Anderson, D. *Z. Kristall.* **1969**, *130*, 148.
(30) Thompson, P.; Cox, D. E.; Hastings, J. B. *J. Appl. Crystallogr.* **1987**, *20*, 79.
(31) Rudolf, P. R.; Clearfield, A. *Inorg. Chem.* **1989**, *28*, 1706.
(32) Louër, M.; Brochu, R.; Louër, D.; Arsalane, S.; Ziyad, M. *Acta Crystallogr.* **1995**, *B51*, 908.
(33) Poojary, D. M.; Shpeizer, B.; Clearfield, A. *J. Chem. Soc., Dalton Trans.* **1995**, *1*, 111.
(34) Bénard, P.; Louër, D.; Dacheux, N.; Brandel, V.; Genet, M. *An. Quim. Int. Ed.* **1996**, *92*, 79.
(35) DeWolff, P. M. *J. Appl. Crystallogr.* **1985**, *1*, 108.

Table 1. Unit Cell Parameters and Details of the Structure Refinement of $KZr_{2-x}U_x(PO_4)_3$ ($x \leq 0.20$) in Space Group $R\bar{3}c$

x (EMPA)	*x* (refined)	R_{wp}, %[b]	R_F, %	χ^2	*a*, Å	c, Å	*V*, Å^3
0	0[a]	10.59	5.47	1.979	8.71128(21)	23.9811(9)	1576.03(8)
0.021(2)	0.020(8)	8.17	4.88	1.539	8.70464(22)	24.0294(8)	1576.79(8)
0.075(4)	0.074(10)	10.40	5.46	1.825	8.71519(22)	24.0224(8)	1580.16(8)
0.102(11)	0.098(10)	10.50	7.25	1.867	8.72094(23)	24.0057(8)	1581.14(8)
0.199(14)	0.196(10)	9.85	7.61	1.727	8.73498(24)	24.0319(8)	1587.97(8)

pattern range (2θ), deg	13−125	P−O distances and tolerance, Å	1.54(4)
step scan increment (2θ), deg	0.02	Zr−O distances and tolerance, Å	2.075(40)
counting time, s	14		

[a] Data collected on a sample mixed with an internal standard. See text for a description of the data collection parameters. [b] For definitions of standard *R* values, see Larson and Von Dreele.[25]

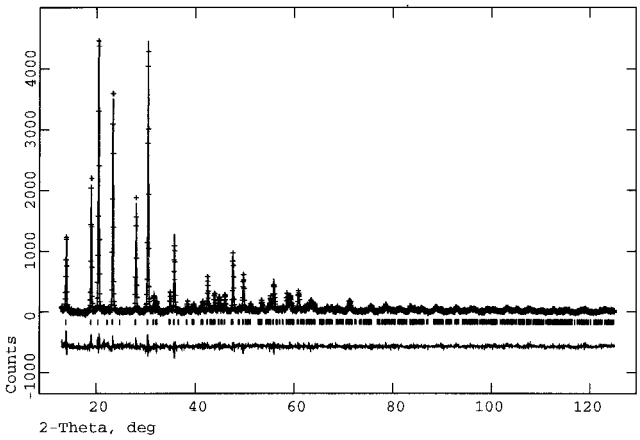

Figure 1. Final observed (+), calculated (full line), and difference profiles for 13−125° 2θ region for $KZr_{1.90}U_{0.10}(PO_4)_3$. Reflections allowed for the space group are marked below the calculated profile.

Table 2. Final Positional and Thermal Parameters (and Esds) for $KZr_2(PO_4)_3$

atom	site sym	*x*	*y*	*z*	U_{iso}, Å^2
Zr	$\bar{3}$	0	0	0.14939(10)	0.0238(8)
K	$\bar{3}$	0	0	0	0.0643(33)
P1	2 (100)	−0.2875(6)	0	$^1/_4$	0.0269(20)
O1	1	0.3044(10)	0.4687(8)	0.26321(26)	0.0179(30)
O2	1	0.1624(7)	0.2051(7)	0.19984(24)	0.0289(35)

Table 3. Final Positional and Thermal Parameters (and Esds) for $KZr_{1.98}U_{0.02}(PO_4)_3$

atom	site sym	*x*	*y*	*z*	U_{iso}, Å^2
U/Zr	$\bar{3}$	0	0	0.14954(6)	0.0271(6)
K	$\bar{3}$	0	0	0	0.0614(19)
P1	2 (100)	−0.2867(4)	0	$^1/_4$	0.0330(15)
O1	1	0.3065(7)	0.4688(5)	0.26305(18)	0.0285(20)
O2	1	0.1631(5)	0.2085(5)	0.19895(19)	0.0327(22)

Table 4. Final Positional and Thermal Parameters (and Esds) for $KZr_{1.93}U_{0.07}(PO_4)_3$

atom	site sym	*x*	*y*	*z*	U_{iso}, Å^2
U/Zr	$\bar{3}$	0	0	0.14939(7)	0.0285(7)
K	$\bar{3}$	0	0	0	0.0707(24)
P1	2 (100)	−0.2879(4)	0	$^1/_4$	0.0362(18)
O1	1	0.3061(8)	0.4688(6)	0.26312(20)	0.0282(24)
O2	1	0.1632(6)	0.2064(6)	0.19940(20)	0.0300(26)

observed data suggested *C*2/*c* or *Cc* symmetry for the $KU_2(PO_4)_3$ unit cell. Therefore, the structure of $KU_2(PO_4)_3$ was determined with the Rietveld method using the *C*2/*c* structure of $KTh_2(PO_4)_3$[14] as a starting model. The phase fraction scale factors, background coefficients, sample displacement error, unit cell parameters, and Lorentzian components of the pseudo-Voigt coefficients

Table 5. Final Positional and Thermal Parameters (and Esds) for $KZr_{1.90}U_{0.10}(PO_4)_3$

atom	site sym	*x*	*y*	*z*	U_{iso}, Å^2
U/Zr	$\bar{3}$	0	0	0.14929(7)	0.0360(7)
K	$\bar{3}$	0	0	0	0.0821(26)
P1	2 (100)	−0.2880(5)	0	$^1/_4$	0.0415(19)
O1	1	0.3055(8)	0.4687(6)	0.26348(21)	0.0345(25)
O2	1	0.1634(6)	0.2050(6)	0.19949(20)	0.0364(27)

Table 6. Final Positional and Thermal Parameters (and Esds) for $KZr_{1.80}U_{0.20}(PO_4)_3$

atom	site sym	*x*	*y*	*z*	U_{iso}, Å^2
U/Zr	$\bar{3}$	0	0	0.14914(7)	0.0446(7)
K	$\bar{3}$	0	0	0	0.0980(28)
P1	2 (100)	−0.2879(5)	0	$^1/_4$	0.0472(20)
O1	1	0.3057(8)	0.4686(6)	0.26367(21)	0.0403(26)
O2	1	0.1634(6)	0.2048(6)	0.19932(20)	0.0380(27)

Table 7. Unit Cell Parameters and Details of the Structure Refinement of $KU_2(PO_4)_3$

space group	*C*2/*c*
a, Å	17.4705(4)
	17.497(5)[a]
b, Å	6.75408(13)
	6.777(2)[a]
c, Å	8.02522(17)
	8.040(3)[a]
β, deg	102.0189(17)
	101.93(1)[a]
V, Å^3	926.196(34)
	932.7(3)[a]
Z	4
pattern ranges (2θ), deg	8−90, 70−139
step scan increments (2θ), deg	0.02, 0.04
counting times, s	7, 14
internal standard *a*, Å	4.15695(6)
P−O distances and tolerance, Å	1.54(4)
U−O distances and tolerance, Å	2.50(25)
R_e, statistically expected R_{wp}, %	10.02
R_{wp}, %	14.07
R_F, %	3.78
χ^2	1.971

[a] Data taken from Keester and Jacobs.[16]

adjusted for strain broadening and peak asymmetry[30] were refined first for each histogram. Soft constraints were applied to the U−O and P−O distances. The atomic positions and thermal parameters were then refined. Removal of the soft constraints in the final stages of the refinement yielded a less chemically realistic structural model. Soft constraints were reapplied and the model converged rapidly with final residuals of $R_{wp} = 14.07\%$, $R_e = 10.02\%$, and $R_F = 3.78\%$.

Table 7 provides details of the structure refinement and experimentally determined unit cell parameters for $KU_2(PO_4)_3$. Unit cell parameters reported in a previous

Table 8. Final Positional and Thermal Parameters (and Esds) for $KU_2(PO_4)_3$

atom	site sym	*x*	*y*	*z*	U_{iso}, Å^2
U	1	0.15370(11)	0.09294(30)	0.03498(22)	0.0088(5)
K	2 (010)	0	0.4018(31)	1/4	0.062(6)
P1	1	0.3089(7)	0.0985(24)	0.3145(14)	0.018(4)
P2	2 (010)	0	−0.0913(32)	1/4	0.015(5)
O1	1	0.0727(11)	0.0384(29)	0.2502(27)	0.008(9)
O2	1	−0.0208(14)	−0.2319(28)	0.0958(26)	0.009(9)
O3	1	0.2238(9)	0.0511(36)	0.3275(28)	0.008(8)
O4	1	0.3600(14)	−0.0905(31)	0.3485(30)	0.021(9)
O5	1	0.2982(14)	0.1454(34)	0.1223(18)	0.014(9)
O6	1	0.3582(17)	0.2424(39)	0.4433(34)	0.050(13)

study[16] are also given for comparison. Atomic positions, thermal parameters, and selected bond distances and angles for $KU_2(PO_4)_3$ are given in Tables 8 and 9.

Spectroscopic Studies. In the UV/vis spectra of compounds of stoichiometry $KZr_{2-x}U_x(PO_4)_3$ ($0 \le x \le 0.20$), the absorption bands are similar in number and position to those in the spectrum of UP_2O_7,[27] in which U(IV) is present in pseudo-octahedral coordination with its nearest neighbors. This similarity suggests an octahedral coordination environment for U(IV) in $KU_{2-x}Zr_x(PO_4)_3$. The UV/vis spectra of $KZr_{2-x}U_x(PO_4)_3$ ($x = 0.20$ and $x = 2$) prepared in alumina crucibles are shown in Figure 2. The absorption bands in the spectrum of $KU_2(PO_4)_3$ are similar in position and number to those in the spectra of other U(IV) phosphates such as $U_2O(PO_4)_2$,[34] in which the U(IV) is present in 7-fold coordination with oxygen; however, the absorption bands in the spectrum of $KU_2(PO_4)_3$ are greater in number and shifted in position to slightly longer wavelengths (lower energies), suggesting that the U(IV) coordination environment in $KU_2(PO_4)_3$ is less symmetric than that for U(IV) in $U_2O(PO_4)_2$. Indeed, U(IV) occupies a special position with C_2 site symmetry in $U_2O(PO_4)_2$ whereas U(IV) occupies a general position with C_1 site symmetry in $KU_2(PO_4)_3$. The complexity of the $KU_2(PO_4)_3$ absorption spectra may be attributed to total splitting of degenerate U(IV) energy levels. The characteristic vibronic absorption bands of U(VI) as UO_2^{2+} are absent in the 350−450 nm region of all of

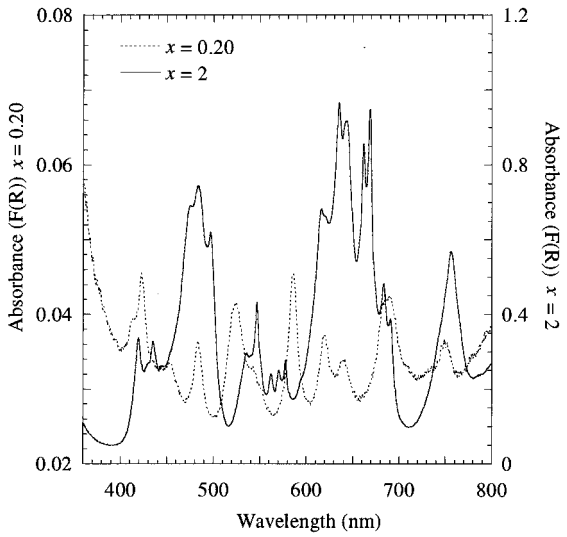

Figure 2. Representative diffuse reflectance spectra of compounds in the series $KZr_{2-x}U_x(PO_4)_3$ ($x = 0.20$ and $x = 2$). The presence of absorption bands in the 400−800 nm regions of the spectra, where forbidden f → f transitions may occur due to vibronic coupling, establishes the presence of U(IV) in the compounds. The spectra of $KZr_{2-x}U_x(PO_4)_3$ ($0 \le x \le 0.20$) are similar to the spectrum of UP_2O_7,[27] in which U(IV) is in pseudo-octahedral coordination with oxygen. The spectrum of $KU_2(PO_4)_3$ is similar to the spectrum of $U_2O(PO_4)_2$,[34] in which the U(IV) coordination is 7-fold. Note the absence of the characteristic vibronic absorption bands of U(VI) (as UO_2^{2+}) in the 350−450 nm regions of the spectra.

Table 9. Selected Bond Distances (Å) and Angles (deg) (and Esds) for $KU_2(PO_4)_3$[a]

		U−O Polyhedron			
U−O1^{i}	2.478(19)	O1^{i}-U−O1^{iv}	106.2(6)	O2^{iii}-U−O5^{i}	148.5(7)
U−O1^{iv}	2.582(22)	O1^{i}-U−O2^{iii}	74.7(8)	O2^{iii}-U−O5^{vii}	84.3(8)
U−O2^{iii}	2.521(23)	O1^{i}-U−O3^{i}	63.6(6)	O2^{iii}-U−O6^{viii}	108.2(8)
U−O3^{i}	2.428(22)	O1^{i}-U−O3^{iv}	148.1(8)	O3^{i}-U−O3^{iv}	112.7(6)
U−O3^{iv}	2.463(18)	O1^{i}-U−O4^{vi}	74.9(7)	O3^{i}-U−O4^{vi}	78.2(8)
U−O4^{vi}	2.366(22)	O1^{i}-U−O5^{i}	121.0(6)	O3^{i}-U−O5^{i}	57.9(5)
U−O5^{i}	2.501(23)	O1^{i}-U−O5^{vii}	141.5(8)	O3^{i}-U−O5^{vii}	115.4(6)
U−O5^{vii}	2.422(19)	O1^{i}-U−O6^{viii}	74.4(9)	O3^{i}-U−O6^{viii}	81.3(8)
U−O6^{viii}	2.386(25)	O1^{iv}-U−O2^{iii}	58.13(24)	O3^{iv}-U−O4^{vi}	136.8(8)
		O1^{iv}-U−O3^{i}	152.8(8)	O3^{iv}-U−O5^{i}	68.3(7)
		O1^{iv}-U−O3^{iv}	61.6(6)	O3^{iv}-U−O5^{vii}	70.2(9)
		O1^{iv}-U−O4^{vi}	125.4(7)	O3^{iv}-U−O6^{viii}	73.8(9)
		O1^{iv}-U−O5^{i}	129.2(6)	O4^{vi}-U−O5^{i}	86.6(7)
		O1^{iv}-U−O5^{vii}	88.6(7)	O4^{vi}-U−O5^{vii}	67.7(8)
		O1^{iv}-U−O6^{viii}	71.6(8)	O4^{vi}-U−O6^{viii}	148.3(9)
		O2^{iii}-U−O3^{i}	132.9(7)	O5^{i}-U−O5^{vii}	66.6(7)
		O2^{iii}-U−O3^{iv}	114.2(6)	O5^{i}-U−O6^{viii}	102.6(8)
		O2^{iii}-U−O4^{vi}	70.6(7)	O5^{vii}-U−O6^{viii}	143.8(9)
		P−O Tetrahedra			
P1−O3^{i}	1.547(9)				
P1−O4^{i}	1.548(9)	O3^{i}-P1−O4^{i}	110.1(19)	O4^{i}-P1−O5^{i}	106.9(15)
P1−O5^{i}	1.547(9)	O3^{i}-P1−O5^{i}	101.0(14)	O4^{i}-P1−O6^{i}	100.4(16)
P1−O6^{i}	1.543(9)	O3^{i}-P1−O6^{i}	119.7(18)	O5^{i}-P1−O6^{i}	118.3(19)
P2−O1^{i}	1.543(7)				
P2−O1^{ii}	1.543(7)	O1^{i}-P1−O1^{ii}	110.8(24)	O1^{ii}-P1−O2^{i}	107.0(11)
P2−O2^{i}	1.542(7)	O1^{i}-P1−O2^{i}	114.0(12)	O1^{ii}-P1−O2^{ii}	114.0(12)
P2−O2^{ii}	1.542(7)	O1^{i}-P1−O2^{ii}	107.0(11)	O2^{i}-P1−O2^{ii}	104.0(24)

[a] Symmetry codes: (i) x, y, z; (ii) $\bar{x}, y, \bar{z} + 1/2$; (iii) $\bar{x}, \bar{y}, \bar{z}$; (iv) $x, \bar{y}, z + 1/2$; (v) $x + 1/2, y + 1/2, z + 1/2$; (vi) $\bar{x} + 1/2, y + 1/2, \bar{z} + 1/2$; (vii) $\bar{x} + 1/2, \bar{y} + 1/2, \bar{z}$; (viii) $\bar{x} + 1/2, \bar{y} + 1/2, z + 1/2$.

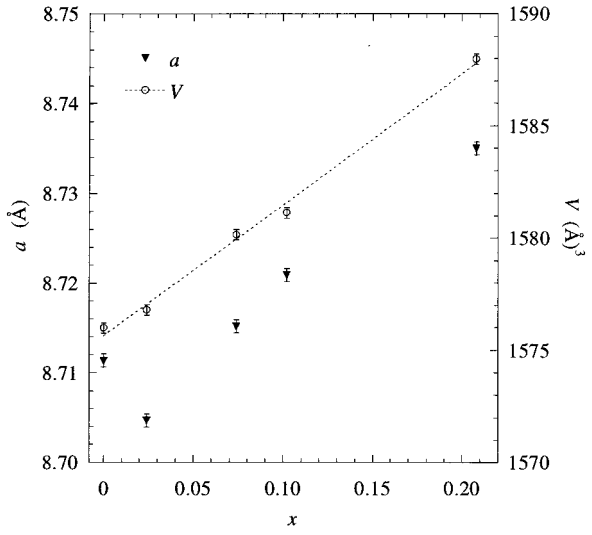

Figure 3. Relationship of hexagonal cell parameters for $KZr_{2-x}U_x(PO_4)_3$ ($x \leq 0.20$), $R\bar{3}c$ compounds that belong to the [NZP] structural family. There is a linear increase in cell volume as the value of x increases. However, there is an unexpected contraction of the a axis for $x = 0.02$ followed by a nearly linear increase its length. The c axis (not shown in the figure) elongates for $x = 0.02$ but thereafter remains essentially unchanged. The error bars are the differences in the Rietveld refined cell parameters of two or more samples of the same composition and are not the statistical uncertainties in the parameters returned by GSAS.

the spectra. The UV/vis spectra of the compounds prepared in alumina crucibles are similar to the spectra of the compounds prepared in glassy carbon crucibles, indicating that either type of crucible is suitable for the synthesis of a U(IV)-bearing compound.

Discussion

When the hexagonal cell parameters of $KZr_{2-x}U_x(PO_4)_3$ ($x \leq 0.20$) obtained from our refinements are compared to those of $KZr_2(PO_4)_3$, an increase in cell volume is observed for increasing values of x. This increase is due to substitution of the larger U^{4+} ($r = 0.89$ Å) for Zr^{4+} ($r = 0.72$ Å)[18] on the octahedrally coordinated A site. An initial decrease in the length of the a axis for $x = 0.02$ is followed by a nearly linear increase in the length of a. This behavior is shown in Figure 3. The length of the c axis increases for $x = 0.02$ but thereafter varies in a nonlinear fashion. The trends of the cell parameters were verified by additional XRD measurements on newly prepared samples of the same composition. The error bars in Figure 3 are the differences in the Rietveld refined cell parameters of two or more samples of the same composition and are not the statistical uncertainties in the parameters returned by GSAS.

The abrupt change in the unit cell parameters of $KZr_{2-x}U_x(PO_4)_3$ ($x = 0.02$) could not be ascribed to a change in cell symmetry resulting from cation ordering on A or M′ or from K^+ occupation of M″. Attempts to refine the powder XRD data for $KZr_{2-x}U_x(PO_4)_3$ ($x = 0.02$) using an $R\bar{3}$ or $C2/c$ structural model[12,36] were unsuccessful. The refinements yielded grossly inflated values for the reliability factors (in the former case) or would not converge (in the latter case). Therefore, the anomalous behavior of the cell parameters of $KZr_{2-x}U_x(PO_4)_3$ for $x = 0.02$ is real and unexplained.

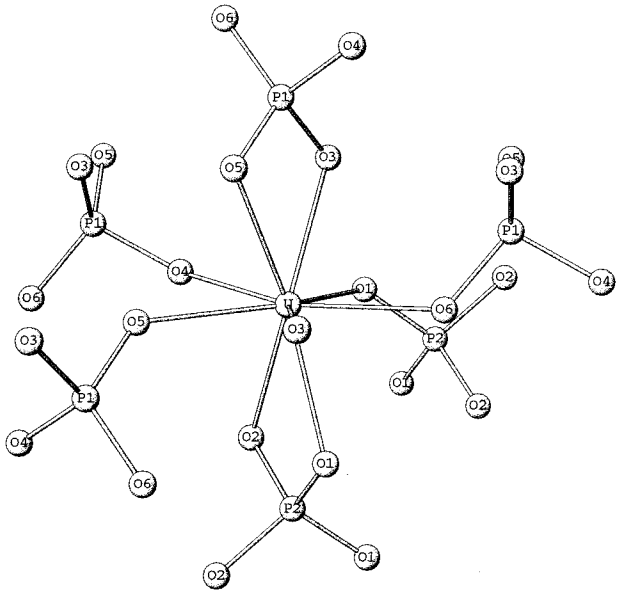

Figure 4. U−O coordination environment in $KU_2(PO_4)_3$. Some atoms have been omitted for clarity. This figure was drawn with ATOMS for WINDOWS (version 4.1, Shape Software).

Our structural and spectroscopic data suggest that $KZr_2(PO_4)_3$ accommodates substitutions of the larger U^{4+} for Zr^{4+} on the octahedrally coordinated A site; however, the solid solubility limit for $KU_2(PO_4)_3$ in $KZr_2(PO_4)_3$ has not been determined. The refined values of x agree well with those determined by our electron microprobe analyses which suggests that all the U(IV) is located on the A site. The data given in Tables 2−6 reflect the structural disorder caused by U^{4+} substitution for Zr^{4+} on A. Note the increase in the mean isotropic thermal parameter of the A site occupants as the value of x increases.

U(IV) Coordination in $KU_{2-x}Zr_x(PO_4)_3$ ($x \leq 0.20$). Octahedral coordination for U(IV) in $KU_{2-x}Zr_x(PO_4)_3$ ($0 \leq x \leq 0.20$), suggested by UV/vis spectra of the compounds, is confirmed by our refined XRD data. The A−O octahedra remain intact as the value of x increases. A−O distances decrease as the value of x increases. O−A−O angles within the octahedra are close to the ideal values of 90° and 180°.[37]

The P−O tetrahedra in each member of $KU_{2-x}Zr_x(PO_4)_3$ ($x \leq 0.20$) are close to ideal with O−P−O angles between 108.1(5)−111.6(5)° and P−O distances between 1.536(4)−1.550(4) Å.[37] As the value of x increases, the A−O−P angles of the $[A_2(PO_4)_3]^-$ anionic framework increase, contributing to the unit cell volume expansion shown in Figure 3.

U(IV) Coordination in $KU_2(PO_4)_3$. The U(IV) coordination polyhedra in $KU_2(PO_4)_3$ involve nine oxygen atoms from seven PO_4 groups. Six oxygen atoms of each U−O polyhedron are shared with three neighboring edge-sharing U−O polyhedra. The U−O coordination polyhedra, as shown in Figure 4, are more irregular

(36) El Jazouli, A.; El Bouari, A.; Fakrane, H.; Housni, A.; Lamire, M.; Mansouri, I.; Olazcuaga, R.; Le Flem, G. *J. Alloys Compd.* **1997**, 49.

(37) Kepert, D. L. *Inorganic Stereochemistry;* Springer-Verlag: Berlin, Germany, 1982.

than either the tricapped trigonal prism or the capped square antiprism with U−O distances between 2.37(2)−2.58(2) Å.[37] As in $KTh_2(PO_4)_3$, the edge-sharing U−O polyhedra form infinite sheets along the *b* and *c* axes of the monoclinic unit cell that are linked by bridging P2−O tetrahedra whose phosphorus atoms lie in special positions on 2-fold axes.[14] K^+ occupy 8-fold interstitial positions along a 2-fold axis between bridging P2−O tetrahedra. The occupation of structural sites between these bridging tetrahedra gives rise to a close-packed, three-dimensional network.

There are two independent, discrete PO_4 groups in the structure: P1−O tetrahedra are surrounded by five U−O polyhedra and act as a bidentate ligand for one of them; P2−O tetrahedra are surrounded by four U−O polyhedra and act as bidentate ligands for two of them.

Relationship of $KU_2(PO_4)_3$ to Compounds of $KA_2(PO_4)_3$ Stoichiometry. Compounds of general stoichiometry $KA_2(PO_4)_3$ in which A = Zr, Hf, Ti, or Ge are rhombohedral and described by hexagonal cell parameters whereas those compounds in which A = U or Th are monoclinic.[14] Therefore, the hexagonal cell parameters of the former compounds[38,39] were recast on a monoclinic cell[40] with the transformation matrix: $a_h = -{}^1/_2a_{mon} - {}^1/_2b_{mon}$, $b_h = {}^1/_2a_{mon} - {}^1/_2b_{mon}$, and $c_h = -a_h - 3c_{mon}$. In Figure 5, we have plotted the monoclinic a_{mon} and c_{mon} unit cell parameters of $KU_2(PO_4)_3$ and compounds of general stoichiometry $KA_2(PO_4)_3$ as a function of the ionic radius of A (r_A). Note the concomitant increase in the length of a_{mon} with the increase in r_A for all $KA_2(PO_4)_3$ compounds. Our experimentally determined unit cell parameters for $KU_2(PO_4)_3$, as shown in Figure 5, are consistent with this trend. Within each structure field ($R\bar{3}c$ or $R\bar{3}$ [NZP] compounds in which the coordination of A is octahedral and $C2/c$ compounds in which the coordination of A is 9-fold), both a_{mon} and c_{mon} increase with an increase in r_A. The linear relation between a_{mon} and r_A ($a_{mon} = 10.106 + (7.055r_A)$) can be used to derive a value for the a_{mon} axis of $KPu_2(PO_4)_3$ in which Pu(IV) is 9-coordinate ($r_A \approx 1.01$ Å; $a_{mon} = 17.2$ Å). Experiments are underway to prepare $KPu_2(PO_4)_3$ and to measure its structural properties.

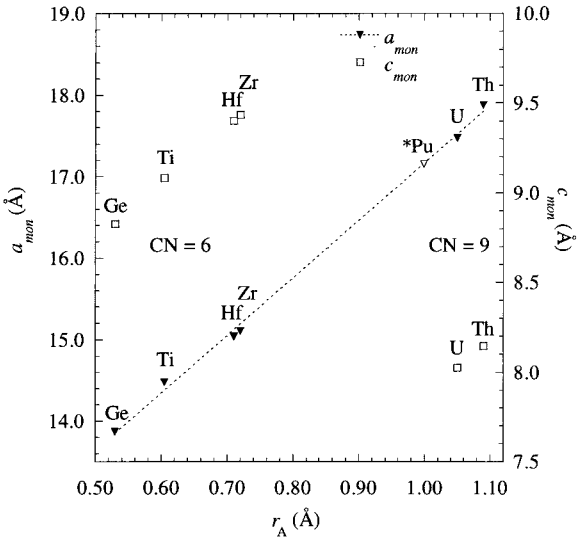

Figure 5. Relationship of $KU_2(PO_4)_3$ to compounds of general stoichiometry $KA_2(PO_4)_3$. The hexagonal cell parameters of compounds $KA_2(PO_4)_3$ in which A = Ti, Zr, Hf, or Ge[38,39] were recast on a monoclinic cell[40] so that the relationship between compounds of general stoichiometry $KA_2(PO_4)_3$ could be determined. A predicted value of a_{mon} for $KPu_2(PO_4)_3$, derived using the linear relation between a_{mon} and r_A, is marked with an asterisk (*Pu).

Acknowledgment. We wish to express our appreciation to C. A. Hijar and E. J. Peterson of LANL for assistance with powder XRD data collection and thoughtful discussions of the results of our Rietveld refinements. We would also like to thank M. P. Wilkerson of LANL, who prepared the UCl_4 powder used in our experiments. Funding for this effort was made possible through the Nuclear Materials Stabilization Task Group, EM-66 of the U. S. Department of Energy under Contract W-7405-ENG-36.

Supporting Information Available: A complete listing of bond distances and angles for $KU_2(PO_4)_3$. This material is available free of charge via the Internet at http://pubs.acs.org.

CM990209F

(38) JCPDS-ICDD files 35-756, 38−1471, and 34−131, PDF-2 Sets 1−46: JCPDS-ICDD: Newtown Square, PA, 1996.

(39) Brochu, R.; Louër, M.; Alami, M.; Alqaraoui, M.; Louër, D. *Mater. Res. Bull.* **1997**, *32*, 113.

(40) Boisen, M. B.; Gibbs, G. V. *Mathematical Crystallography;* The Mineralogy Society of America: Washington, DC, 1985.